Ceramics International 46 (2020) 12613–12617

Contents lists available at ScienceDirect

Ceramics International

journal homepage: www.elsevier.com/locate/ceramint

Accurate residual stress measurement as a function of depth in environmental barrier coatings via a combination of X-ray diffraction and Raman spectroscopy

Cheng Ye, Peng Jiang*

State Key Laboratory for Strength and Vibration of Mechanical Structures, School of Aerospace Engineering, Xi'an Jiaotong University, Xi'an, 710049, China

ARTICLE INFO

Keywords:
Environmental barrier coating
Residual stress
X-ray diffraction
Laser Raman spectroscopy

ABSTRACT

This study examined the properties of the latest generation of rare earth silicate environmental barrier coating system (EBCs). By combining X-ray diffraction and Raman spectroscopy, a novel and efficient method was developed to measure residual stress in EBCs produced by slurry coating. A 633-nm-wavelength laser beam from the confocal microlaser of a Raman spectrometer was focused on the cross-section of samples, and the spectra were recorded. We performed non-linear multi-peak spectrum fitting with the Lorenz function to obtain the peak shift of the EBC top coat at 5 μm intervals as a function of depth. We then obtained the stress distribution along the depth by calibrating the stress value on the surface via X-ray diffraction. The residual stress in the coating which endured high temperature, water, and oxygen corrosion without serious damage, was non-uniform and compressive. The stress at the bottom of the coating was approximately −275 MPa, decreasing towards the surface. A sudden shift in stress value was observed in the distribution of the residual stress, which was attributed to residual stress relaxation caused by microscopic pores contained within the coating.

1. Introduction

SiC-based ceramic matrix composites (CMC-SiCs) are high-temperature-resistant structural composite materials with excellent practical properties. These materials have been widely used in high-temperature environments, and compared to high-temperature alloys, can tolerate higher temperatures while also exhibiting lower density. Thus, they have broad application potential in next-generation gas turbines [1–5]. As CMC-SiCs would be seriously corroded by the high-temperature, water, and oxygen within the gas turbine [6,7], environmental barrier coatings (EBCs) were developed to prevent rapid structural failure [8]. Typical EBCs, similar to thermal barrier coatings (TBCs), consist of a ceramic top coat, thermally grown oxide (TGO), bond coat, and substrate. The initiation and expansion of cracks in the coating ultimately result in the direct contact between the external environment and the internal protected matrix [8,9], and the residual stress from this process is closely linked to the crack behaviour, playing a key role in the failure mechanisms of the coating structure [10,11]. This necessitates the accurate characterisation of the residual stress distribution along the depth dimension of the EBC top coat.

Currently, there are few methods for measuring residual stress in an EBC system, and X-ray diffraction (XRD) [12] is one such commonly used method. However, to isolate the environment from the protected substrate, the top coat is generally very dense, thus limiting the penetration depth of conventional X-rays. Therefore, it is not possible to measure the stress distribution across the approximately 80-μm-thick coating employing this approach. Moreover, even if the penetration depth was sufficient, the stress values at specific depths could not be discerned. Some studies [13,14] have employed high-energy X-rays to penetrate cylindrical and bulk specimens to measure the residual stress distribution in thermal barrier coatings (TBCs). However, X-ray spot size is as small as about 40 μm generally. The size of the X-ray beam is too large for the thin top coat in EBCs, and the low spatial resolution means that only a small number of data points can be obtained from measurements along the depth of the coating, making it difficult to accurately describe residual stress distribution in the thin coating. Moreover, high-energy X-ray equipment is not commonplace, and its operation and implementation are unpractical.

Laser Raman spectroscopy [15–17] is another common method used for residual stress measurements. The residual stress can be calculated by measuring the peak shift of spectrum. However, the correlation coefficient between the peak shift and stress is influenced by many

* Corresponding author. State Key Laboratory for Strength and Vibration of Mechanical Structures, School of Aerospace Engineering, Xi'an Jiaotong University, No. 28 Xianning West Road, Xi'an, Shaanxi, 710049, PR China.
E-mail addresses: yecwizards@mail.xjtu.edu.cn (C. Ye), jiangpeng219@mail.xjtu.edu.cn (P. Jiang).

https://doi.org/10.1016/j.ceramint.2020.02.025
Received 29 December 2019; Received in revised form 2 February 2020; Accepted 3 February 2020
Available online 04 February 2020

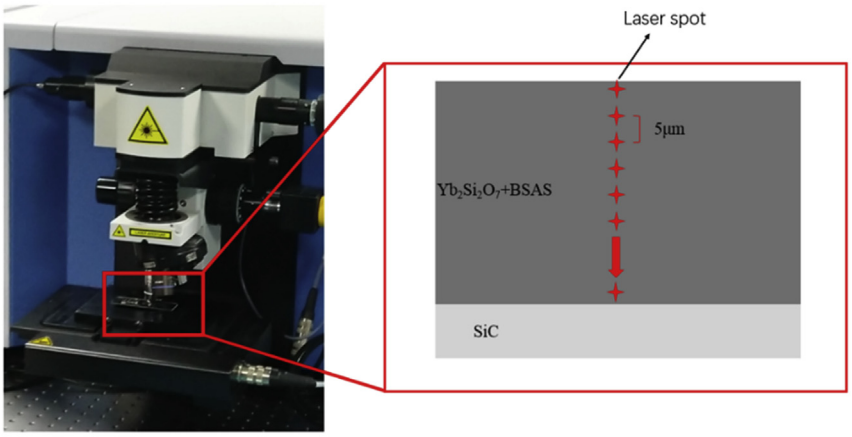

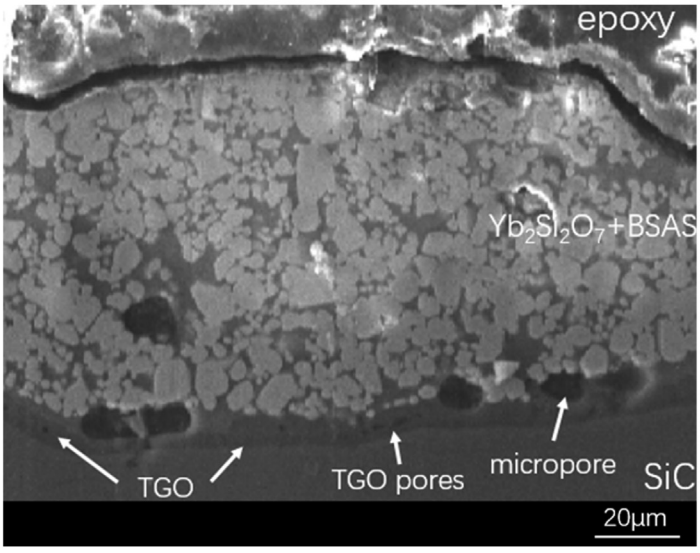

Fig. 1. a) Schematic diagram showing the main steps in Raman spectroscopy measurement process. **b)** SEM of EBC after heat treatment at 1250 ˚C for 50 h showing the special granular microstructure.
The cross-section of the coating was placed under confocal microscope. The red marks represent different positions of the laser irradiated on the coating. The white particles densely covered in the coating area is YbDS while the dark grey gap between particles is BSAS. There are individual micropores produced during manufacture process of EBC. TGO with dense structure and uniform thickness appeared at the interface between the top layer and the bonding layer. The pores in TGO may be related to the chemical reaction between water vapour and TGO. (For interpretation of the references to colour in this figure legend, the reader is referred to the Web version of this article.)

factors, such as microstructure or heat treatment parameters. Moreover, its value is not constant as it is inherently material-related. Therefore, the correlation coefficients of different batches of samples may be different from one another, resulting in a method that is troublesome and difficult to calibrate. Near-field photoluminescence [18,19] has allowed for high spatial resolution measurements of residual stress in the TGO of TBCs with high measurement accuracy. However, as with X-rays, the penetration depth of the laser into the EBCs was insufficient, and the materials employed to manufacture EBCs do not possess photoluminescence properties.

To overcome these difficulties, we coupled the XRD method with laser Raman spectroscopy to consolidate the strengths of both approaches, thereby accurately measuring the residual stress distribution in sample sections; afterwards, the data was post-processed to compensate for the stress release effect caused by the sectioning.

2. Experimental procedure

2.1. Coating material and experimental equipment

The EBCs used in this study were prepared by the slurry coating method at Northwestern Polytechnical University. Two dimensional C/SiC composites substrates (40 × 5 × 3.5 mm) were produced via chemical vapour infiltration (CVI). A 40 μm thick layer of SiC was deposited on the surface of the sample as the bond coat of the EBC. The components of the 80-μm-thick top coat were $Yb_2Si_2O_7$ (i.e. “YbDS”, for short) and $Ba_{0.5}Sr_{0.5}Al_2Si_2O_8$ (i.e. “BSAS”, for short). The main purpose of adding BSAS with a mass fraction of 10% was to lower the temperature required for coating sintering. The samples were placed in an aluminium oxide tube furnace to simulate a high-temperature and corrosive environment containing 50% water vapour and 50% oxygen for 50 h at 1250 ˚C. Then, the samples were wrapped in resin and cut into 10 × 5 × 3.5 mm cross-section pieces with a diamond wire saw to measure the residual stress. The downward cutting speed of the diamond wire was set to 3 mm per hour. Laser Raman spectra were collected using a confocal micro-laser Raman spectrometer (LabRAM HR Evolution, HORIBA). The minimum measurement resolution of this instrument is as high as 1 μm. Measurements of residual surface stress via XRD were also carried out with an X-ray diffractometer (Bruker D8 advance).

2.2. Raman spectroscopy for stress measurement in top coat

YbDS was used to characterise the stress state within the coating, given that it was the main coating component. The Raman spectra were acquired as indicated in Fig. 1a. The He/Ne laser operating at 633 nm

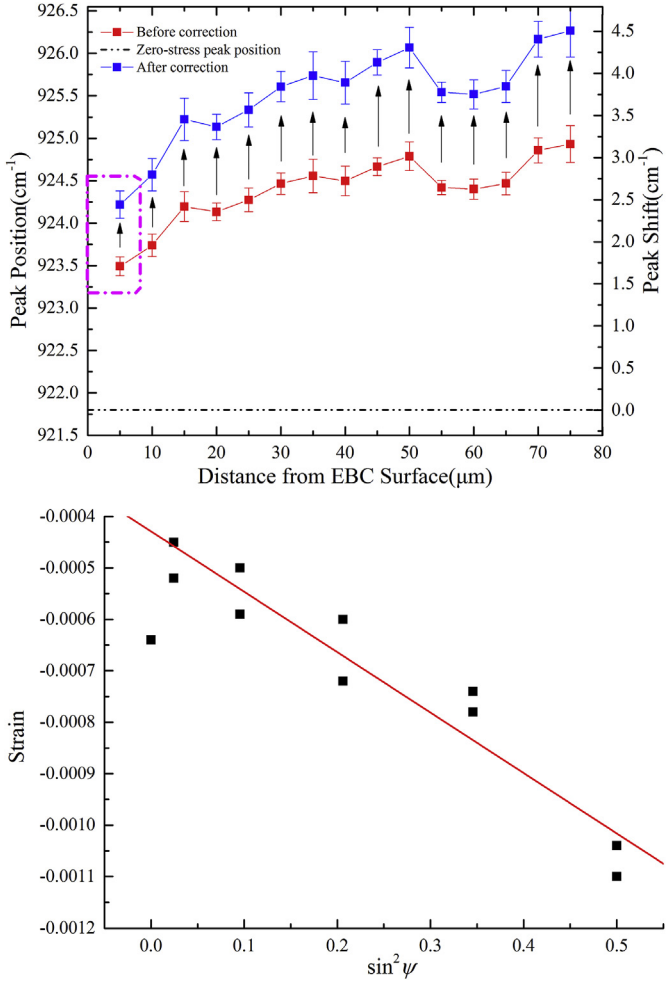

Fig. 2. a). The Raman peak shifts measured on cross-sections along the coating depth **b)** XRD surface stress measurement data.
The corrected peak positions represent the stress distribution inside the coating before sectioning. The pink pane represents the approximate penetration depth of XRD, in which peak shift data was used to calculate PS coefficient. The stress values corresponding to this data was from the strain versus sin^2 ψ plot obtained by XRD stress measurement. (For interpretation of the references to colour in this figure legend, the reader is referred to the Web version of this article.)

was irradiated on the cross-section of the top coat and Raman spectra were recorded by a detector integrated into the microscopes. The measured points were evenly distributed at intervals of 5 μm from the surface of the top coat to the interface between the top coat and TGO, and three different positions were measured at the same depth to calculate the standard deviation. Additionally, as the morphology of the top layer was not perfectly uniform, the measurements were performed exclusively in the YbDS areas which occupied the majority of the surface and were characteristically bright coloured, rather than in the grey and scattered BSAS portions.

To reduce measurement errors caused by rising temperatures [20] and to obtain a good signal-to-noise ratio and peak intensity, the He/Ne laser power was set to 25% of its maximum value. Afterwards, a single measurement point was scanned five times, each time for 5 s at a fully controlled temperature (298 ± 1 K) in ambient air. To accurately determine the exact location of Raman peaks, the recorded spectra were smoothed and denoised, after which multi-peak fitting was performed via the Labspec5 software included with the instrument. In Raman spectroscopy, Lorentz analysis is typically used to fit the peaks of crystals. Similarly, the materials used in this study were also crystals such as YbDS, BSAS and even TGO; thus, Lorenz peak fitting was selected for multi-peak fitting to obtain exact Raman peak positions.

2.3. X-ray diffraction for stress measurement on top coat surface

The XRD method used in this paper is widely known as the sin^2 ψ method, which is also based on the measurement of peak shift in the XRD pattern recorded at different ψ angles, similar to Raman piezo-spectroscopy. In this method, a specific diffraction plane is selected first and the lattice parameters are measured by a coupled θ - 2θ scan at different tilt angles of the sample. All XRD measurements were carried out using the Bruker D8 advance system equipped with a Cu target. The [$\bar{2}$20] plane was selected due to its relatively strong intensity, in addition to the fact that higher 2θ peaks have much lower intensities and irregular shapes. Moreover, a higher 2θ angle would be indicative of higher X-ray penetration depth, which would expand the area of XRD measurement and affect the accuracy of the stress values eventually. Regarding lower 2θ peaks, the signal-to-noise ratio of diffraction data is too low, which leads to a higher measurement error. The detector scanned in the 2θ ranges from 40 to 55 to measure the [$\bar{2}$20] peaks (2θ = 47.700). Only the residual stress on the surface region of the coating was measured without considering the information on the cross-section region. The sin^2 ψ plot used to calculate stress was taken from the same sample measured in the Raman spectrum experiment.

3. Experimental results and discussion

3.1. In-plane residual stress distribution trend in top coat

The microstructure of the YbDS/BSAS top coat after heat treatment is presented in Fig. 1b. The top coat is thinner than a typical TBC, with a uniform surface covered with bright and grey areas. Importantly, no large cracks were observed, which indicated the good protective performance of the coating. Moreover, the darker TGO layer is visible in the SEM image.

The distribution of residual stress through the thickness of coatings has been measured by Raman piezo-spectroscopy. For cubic crystal systems, the relationship between stress and peak shifts can be expressed as follows [21]:

$$\Delta\nu_n = \frac{\Pi_n(\sigma_1 + \sigma_2 + \sigma_3)}{3} \quad (1)$$

where the subscript n refers to the Raman peak, and ν refers to peak shifts. However, the crystal structure of YbDS belongs to the monoclinic system instead of the cubic crystal system. Many well-formed, symmetrical peaks with high intensity and a narrow FWHM (i.e. full width at half maximum) appeared in the spectrum. According to previous literature [22], the peak with the highest intensity at approximately 921 cm^{-1} corresponds to the characteristic peak of Si–O–Si bend vibration in a silicon-oxygen tetrahedron. Considering that the distinctive minimal lattice distortion of the silicon-oxygen tetrahedron structure is observed in YbDS crystals due to its high structural stiffness [23], the cubic structure of YbDS facilitated the calculation of residual stress through Equation (1). Here, we observed a significant linear relationship between the characteristic peak shift at 921 cm^{-1} and the applied stress.

The red data in Fig. 2 indicate the distribution of Raman peak positions and shifts along the depth of the coating after sectioning, which were obtained by performing a series of experimental measurements on polished cross-sections as described in Fig. 1a. An example of data processing for multi-peak Lorenz fitting is given in Fig. 3. The fitting curves and spectrums coincide almost perfectly, with an R-squared value of 0.97.

The stress-free Raman peak position of YbDS was determined on spectra from stress-free powder from the same batch. All peak shifts were positive in the top coat, indicating that the entire coating was

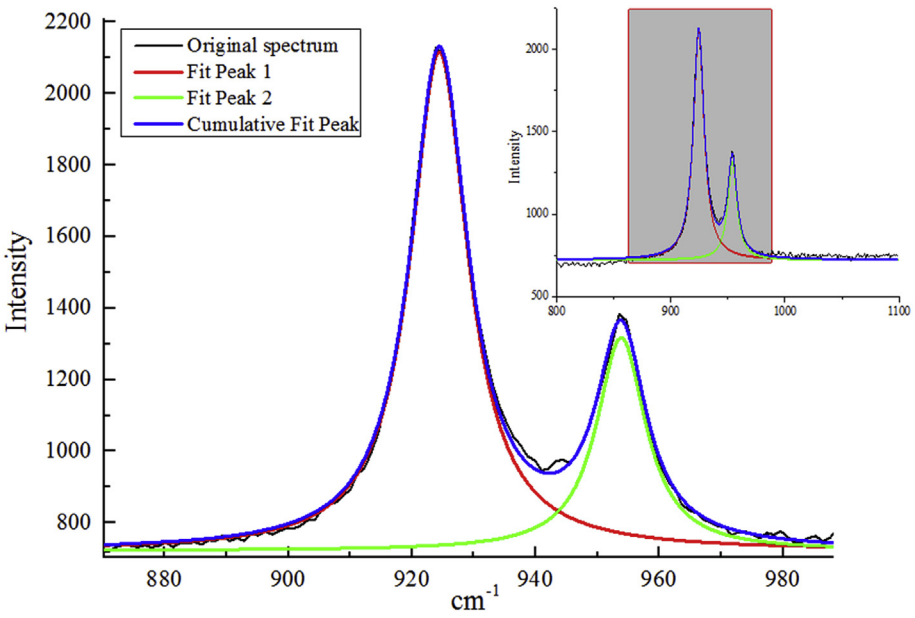

Fig. 3. Original Raman spectrum from certain depth and fitting curves. The image in the upper right corner shows the spectrum before enlargement, where the grey rectangle represents the enlarged area. The Raman peaks at 921 cm^{-1} and 955 cm^{-1} were fitted by the red and green Lorenz curve respectively. The cumulative fitting peaks coincide almost perfectly with the original spectrum, showing high accuracy of peak shift measurement. (For interpretation of the references to colour in this figure legend, the reader is referred to the Web version of this article.)

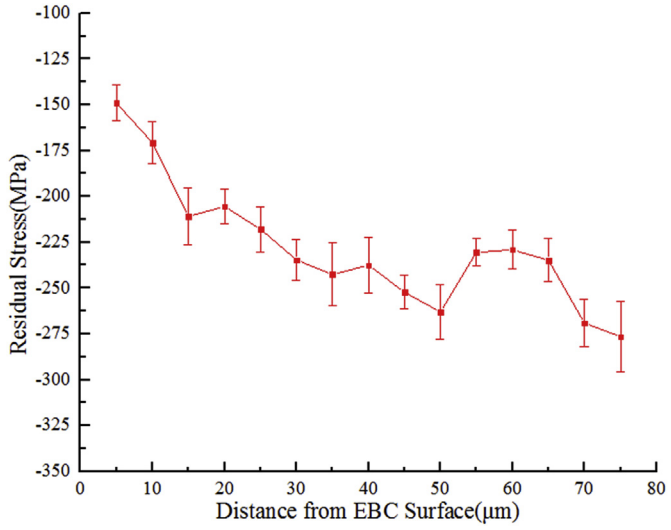

Fig. 4. Distribution of residual stress along the depth of the coating. Similar compressive stress distribution is observed in other samples after heat treatment.

subjected to compressive stress. This is because the coefficient of thermal expansion of SiC is larger than that of YbDS. This conclusion is consistent with the results as well as with previous findings [24]. In previous literature [15], several instances have described approaches to convert the peak shift measured on a cross-section into a measure of the in-plane stress level. The residual stress within the coating before sectioning is equibiaxial (σ_B). After sectioning, the normal stress on the new surface is zero. The strain on the new surface parallel to the cross-section is considered to be the same as before sectioning because samples were completely wrapped with hard resin. Here, the Poisson effect converts the stress at the cross-section (σ_{edge}) to uniaxial stress [σ_B (1-ν)]. Thus, the in-plane stress without sectioning is expressed as $\sigma_B = \sigma_{edge}/(1-\nu)$. Due to the linear relationship between peak shift and applied stress, the same effect was achieved for stress correction by peak shift correction. The peak shift distribution corresponding to in-plane residual stress σ_B along the depth of the coating is indicated as blue data in Fig. 3.

3.2. Exact value of in-plane residual stress in top coat

A residual stress distribution trend can be observed in the coating, but the value of residual stress is not known due to the unknown PS (piezo-spectroscopic) coefficient (Π). Moreover, determining this parameter in YbDS is time-consuming and tedious. In the process of calibrating the PS coefficient, it is necessary to design and manufacture loading fixture by ourselves, prepare block standard sample and other preliminary preparation steps, which is very time-consuming. In addition, since the coefficient itself is not an invariable constant, and is susceptible to the influence of various external factors and the changes of the material itself, the calibrated results are often not universally applicable, which means that every time the stress measurement by Raman spectroscopy needs to re-calibrate the correlation coefficient. Therefore, additional measurements were required to calibrate the stress level, which were obtained with XRD. Thus, we determined that the magnitude of stress near the surface is approximately −149 MPa, shown in Fig. 2. Then, by comparing the stress with the shift of the first data point, we obtained the piezo-spectroscopic coefficient so that in-plane residual stress at other depths could be calculated directly according to the same constant coefficient, as shown in Fig. 4. After the samples were exposed to high temperature water and oxygen environment for 50 h, when the distance from the surface of the top coat was smaller than 50 μm, the residual in-plane compressive stress increased rapidly with the increased distance. Then, the value of residual stress decreased slightly, after which it rose again with a smaller gradient than previously. The stress value reached a maximum of approximately −275 MPa at the interface between the top and bond coat. A similar value [24] was reported by Richards who used the finite element method to calculate residual stresses in coatings after thermal cycling. The difference between the results is due to the smaller thickness and denser morphology of the coating in our study. This non-uniform behaviour was also observed in Li's research [14] on TBCs. The microscopic pores existing in the coating are the likely cause of a certain degree of stress release.

Our distinctive approach combining Raman spectroscopy with XRD can ingeniously skip the traditional process of calibrating PS coefficients to avoid the disadvantages of Raman spectroscopy, saving time and ensuring outstanding accuracy. Moreover, all instruments used herein are easy to acquire and to operate, which leads to high efficiency in measurement. However, to guarantee the feasibility of this approach, we must ensure that the PS coefficient in the entire coating remains

constant and does not vary with depth. As reported by Limarga et al. [16,25], the phase transformation of materials can also cause the shift of Raman peaks, which will affect the PS coefficient. According to the Raman spectrum at each depth measured before, no impure peaks were found except the obvious characteristic peaks of YbDS, confirming that there are no high-temperature phase transformations in YbDS.

Additionally, since surface stress was measured by XRD and the first data point with a depth of 5 μm was evaluated to confirm the PS coefficient, it must be clear whether the two can reasonably match. When X-ray is irradiated onto a surface at θ angle (23.50°), the penetration depth τ of it can be expressed by the Beer-Lambert Law: $I/I_0 = e^{-\mu\tau/\sin\theta}$, where θ is the angle of incidence, I and I_0 are the intensity of the X-ray after and before penetration, μ is the linear attenuation coefficient which can be estimated by $\mu \approx k\rho Z^3\lambda^3$, in which the physical quantities from left to right are the density, the atomic number of materials, and the wavelength of the X-ray, respectively. By substitution of the related physical quantities into these expressions, it was found that the X-ray can only penetrate the outermost layer with a thickness of approximately 7 μm of the YbDS coating, and therefore it is reasonable to match the surface stress with the peak shift at depths of 5 μm. If matching errors must be smaller, more measuring points can be set up in the outermost layer to more accurately obtain the peak shift corresponding to the stress, which should not be time-consuming.

4. Conclusions

In summary, our method for residual stress measurement is largely based on Raman spectroscopy, and thus inherits all of its advantages. The novelty of our approach lies in using XRD to forgo the time-consuming process of calibrating the PS coefficient. Moreover, the fact that the PS coefficient is influenced by microstructure or heat treatment parameters can be compensated by measuring the stress value for each sample to be tested. This method is not only applicable to the materials mentioned in our study, and can be applied to measure the distribution of residual stress in other ceramic or crystalline materials such TBC coatings and semiconductor materials.

Declaration of competing interest

The authors declare that they have no known competing financial interests or personal relationships that could have appeared to influence the work reported in this paper.

Acknowledgement

This work was supported by National Natural Science Foundation of China (11902240), the fund of State Key Laboratory of Long-life High Temperature Materials and the Fundamental Research Funds for the Central Universities.

References

[1] M. Belmonte, Advanced ceramic materials for high temperature applications, Adv. Eng. Mater. 8 (2006) 693–703, https://doi.org/10.1002/adem.200500269 8.
[2] S. Schmidt, S. Beyer, H. Knabe, H. Immich, R. Meistring, A. Gessler, Advanced ceramic matrix composite materials for current and future propulsion technology applications, Acta Astronaut. 55 (3–9) (2004) 409–420, https://doi.org/10.1016/j.actaastro.2004.05.052.
[3] A. Hasegawa, A. Kohyama, R.H. Jones, L.L. Snead, B. Riccardi, P. Fenici, Critical issues and current status of SiC/SiC composites for fusion, J. Nucl. Mater. 283–287 (2000) 128–137, https://doi.org/10.1016/S0022-3115(00)00374-3 00.
[4] H. Ohnabe, S. Masaki, M. Onozuka, K. Miyahara, T. Sasa, Potential application of ceramic matrix composites to aero-engine components, Composites Part A Applied Science & Manufacturing 30 (4) (1999) 489–496, https://doi.org/10.1016/S1359-835X(98)00139-0.
[5] R. Raj, Fundamental research in structural ceramics for service near 2000°C, J. Am. Ceram. Soc. 76 (9) (1993) 2147–2174, https://doi.org/10.1111/j.1151-2916.1993.tb07750.x.
[6] N.S. Jacobson, E.J. Opila, K.N. Lee, Oxidation and corrosion of ceramics and ceramic matrix composites, Curr. Opin. Solid State Mater. Sci. 5 (4) (2001) 301–309, https://doi.org/10.1016/S1359-0286(01)00009-2.
[7] E.J. Opila, Variation of the oxidation rate of silicon carbide with water-vapor pressure, J. Am. Ceram. Soc. 82 (3) (1999) 625–636, https://doi.org/10.1111/j.1151-2916.1999.tb01810.x.
[8] K.N. Lee, Current status of environmental barrier coatings for Si-Based ceramics, Surf. Coating. Technol. 133–134 (11) (2000) 1–7, https://doi.org/10.1016/S0257-8972(00)00889-6.
[9] B.T. Richards, S. Sehr, F.D. Franqueville, M.R. Begley, H.N.G. Wadley, Fracture mechanisms of ytterbium monosilicate environmental barrier coatings during cyclic thermal exposure, Acta Mater. 103 (2016) 448–460, https://doi.org/10.1016/j.actamat.2015.10.019.
[10] B.J. Harder, J.D. Almer, C.M. Weyant, K.N. Lee, K.T. Faber, Residual stress analysis of multilayer environmental barrier coatings, J. Am. Ceram. Soc. 92 (2) (2009) 452–459, https://doi.org/10.1111/j.1551-2916.2008.02888.x.
[11] K.N. Lee, J.I. Eldridge, R.C. Robinson, Residual stresses and their effects on the durability of environmental barrier coatings for SiC ceramics, J. Am. Ceram. Soc. 88 (12) (2005) 3483–3488, https://doi.org/10.1111/j.1551-2916.2005.00640.x.
[12] Q. Chen, W.G. Mao, Y.C. Zhou, C. Lu, Effect of Young's modulus evolution on residual stress measurement of thermal barrier coatings by X-ray diffraction, Appl. Surf. Sci. 256 (23) (2010) 7311–7315, https://doi.org/10.1016/j.apsusc.2010.05.071.
[13] K. Knipe, M.A. Nd, S.F. Siddiqui, C. Meid, J. Wischek, J. Okasinski, J. Almer, A.M. Karlsson, M. Bartsch, S. Raghavan, Strain response of thermal barrier coatings captured under extreme engine environments through synchrotron X-ray diffraction, Nat. Commun. 5 (5) (2014) 4559, https://doi.org/10.1038/ncomms5559.
[14] C. Li, S.D.M. Jacques, Y. Chen, P. Xiao, A.M. Beale, R.J. Cernik, Precise strain profile measurement as a function of depth in thermal barrier coatings using high energy synchrotron X-rays, Scripta Mater. 113 (2016) 122–126, https://doi.org/10.1016/j.scriptamat.2015.10.032.
[15] S. Krämer, S. Faulhaber, M. Chambers, D.R. Clarke, C.G. Levi, J.W. Hutchinson, A.G. Evans, Mechanisms of cracking and delamination within thick thermal barrier systems in aero-engines subject to calcium-magnesium-alumino-silicate (CMAS) penetration, Mater. Sci. Eng. A 490 (1) (2008) 26–35, https://doi.org/10.1016/j.msea.2008.01.006.
[16] A.M. Limarga, R. Vaßen, D.R. Clarke, Stress distributions in plasma-sprayed thermal barrier coatings under thermal cycling in a temperature gradient, J. Appl. Mech. 78 (1) (2011) 1–26, https://doi.org/10.1115/1.4002209.
[17] M. Tanaka, M. Hasegawa, A.F. Dericioglu, Y. Kagawa, Measurement of residual stress in air plasma-sprayed Y2O3–ZrO2 thermal barrier coating system using micro-Raman spectroscopy, Mater. Sci. Eng. A 419 (1–2) (2006) 262–268, https://doi.org/10.1016/j.msea.2005.12.034.
[18] J. Peng, X. Fan, Y. Sun, H. Wang, L. Su, T. Wang, Thermal-cycle dependent residual stress within the crack-susceptible zone in thermal barrier coating system, J. Am. Ceram. Soc. 101 (2018) 4256–4261, https://doi.org/10.1111/jace.15699.
[19] T. Tomimatsu, S.J. Zhu, Y. Kagawa, Local stress distribution in thermally-grown-oxide layer by near-field optical microscopy, Scripta Mater. 50 (1) (2004) 137–141, https://doi.org/10.1016/j.scriptamat.2003.09.005.
[20] S. Kouteva-Arguirova, W. Seifert, M. Kittler, J. Reif, Raman measurement of stress distribution in multicrystalline silicon materials, Mater. Sci. Eng., B 102 (1–3) (2003) 37–42, https://doi.org/10.1016/S0921-5107(02)00744-4.
[21] P. Bouvier, G. Lucazeau, Raman spectra and vibrational analysis of nanometric tetragonal zirconia under high pressure, J. Phys. Chem. Solid. 61 (4) (2000) 569–578, https://doi.org/10.1016/S0022-3697(99)00242-5.
[22] L. Zheng, G. Zhao, C. Yan, X. Xu, L. Su, Y. Dong, J. Xu, Raman spectroscopic investigation of pure and ytterbium-doped rare earth silicate crystals, J. Raman Spectrosc. 38 (11) (2007) 1421–1428, https://doi.org/10.1002/jrs.1789.
[23] C. Xie, J.G. Du, Y.J. Cui, Z. Chen, W.B. Zhang, L. Yi, L. Deng, Variation of Raman spectra of oligoclase under 1.04.4 GPa, Spectrosc. Spectr. Anal. 32 (3) (2012) 691–694 https://doi/10.3964/j.issn.1000-0593(2012)03-0691-04.
[24] B.T. Richards, K.A. Young, F.D. Francqueville, S. Sehr, M.R. Begley, H.N.G. Wadley, Fracture mechanisms of ytterbium monosilicate environmental barrier coatings during cyclic thermal exposure, Acta Mater. 106 (2016) 1–14, https://doi.org/10.1016/j.actamat.2015.10.019.
[25] A.M. Limarga, J. Iveland, M. Gentleman, D.M. Lipkin, D.R. Clarke, The use of Larson–Miller parameters to monitor the evolution of Raman lines of tetragonal zirconia with high temperature aging, Acta Mater. 59 (3) (2011) 1162–1167, https://doi.org/10.1016/j.actamat.2010.10.049.